Universiteit
Leiden
The Netherlands

Fermions and bosons : excitons in strongly correlated materials

Rademaker, L.

Citation

Rademaker, L. (2013, December 11). *Fermions and bosons : excitons in strongly correlated materials*. *Casimir PhD Series*. Retrieved from https://hdl.handle.net/1887/22839

Version:	Not Applicable (or Unknown)
License:	Leiden University Non-exclusive license
Downloaded from:	https://hdl.handle.net/1887/22839

Note: To cite this publication please use the final published version (if applicable).

Cover Page

Universiteit Leiden

The handle http://hdl.handle.net/1887/22839 holds various files of this Leiden University dissertation.

Author: Rademaker, Louk
Title: Fermions and bosons : excitons in strongly correlated materials
Issue Date: 2013-12-11

3
Fermionic models of correlated bilayers

Many properties of an exciton condensate can be deduced by considering the phenomenological Ginzburg-Landau free energy. However, to find specific susceptibilities that match experiments we need a microscopic model, starting with the basic constituents of a correlated bilayer: electrons, holes, and their interactions.

We introduce the fermionic Hubbard model, a remarkably elegant model that still torments many theoretical physicists. Within the mean field theory picture it is easy to discover exciton condensation, as demonstrated in section 3.2. However, the cuprate family that we study has strong interactions and mean-field theory is at best uncontrolled, and at worst completely wrong. We therefore perform a numerical study using the Determinant Quantum Monte Carlo approach, with limitations rooted in the fermion sign problem.

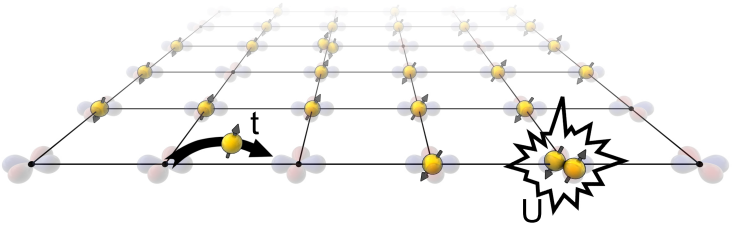

Figure 3.1: In the tight binding approximation the electron states are given by orbitals on an ionic lattice. The dynamics of the electrons is described by the Hubbard model, with hopping t and an onsite repulsion U.

3.1 The Hubbard model and its problems

Many metals and alloys such as the cuprates are crystalline solids, for which most electronic properties can be derived using the tight-binding approximation. There one assumes that the electron wavefunctions are still atomic orbitals and electrons can 'hop' from

A good introduction into the Hubbard model can be found in Zaanen, 1996 and Imada et al., 1998.

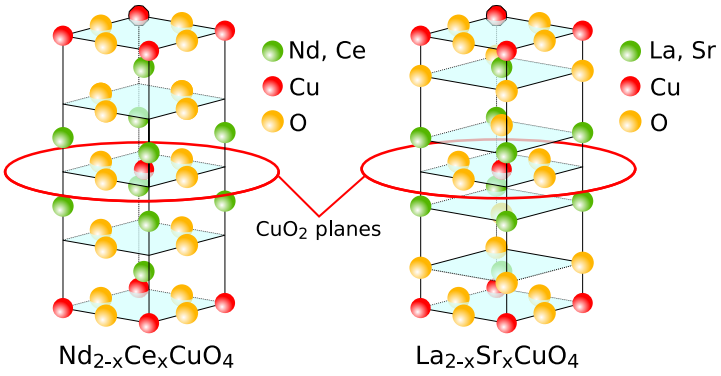

Figure 3.2: Lattice structure of electron and hole-doped cuprates. The interesting physics happens in copper oxide planes, with rare earth ions in between the layers. Doping is obtained by chemical changes in the rare earth layers.

one orbital to the other. This process is described by a **hopping Hamiltonian**

$$H_K = -\sum_{ij\sigma} t_{ij} c^\dagger_{i\sigma} c_{j\sigma} \tag{3.1}$$

where $c^\dagger_{i\sigma}$ creates an electron at site i with spin σ and t_{ij} is the overlap between two atomic orbitals. With the addition of a chemical potential μ, which tunes the electron density, this model represents the simple **Fermi gas**. A Fourier transformation turns the Hamiltonian into a diagonal form in momentum space,

$$H_{\text{FG}} = \sum_{\mathbf{k}\sigma} (\varepsilon_{\mathbf{k}} - \mu)\, c^\dagger_{\mathbf{k}\sigma} c_{\mathbf{k}\sigma} \tag{3.2}$$

where $\varepsilon_{\mathbf{k}}$ is the Fourier transform of t_{ij} and is called the dispersion. We find that the ground state is an **antisymmetrized product state**, which can be viewed as a marginal extension of the classical condensates mentioned in the introduction.

Next to the hopping, which is associated with kinetic energy, there exist interactions between the electrons.[1] This is typically a density-density interaction of the form $V(r - r')n(r)n(r')$, where $V(r)$ is the (screened) Coulomb potential and $n(r) = c^\dagger(r)c(r)$ is the electron density. Landau[2] famously showed that when one slowly turns on these interactions, there remains a one-to-one correspondence between the ground state and excitations of the Fermi gas and the **Fermi liquid**. This principle of adiabatic continuation allows us to neglect electron-electron interactions (or at most treat them perturbatively) in most metals and semiconductors.

[1] There also exist ion-ion interactions and electron-ion interactions, which are commonly referred to as electron-phonon coupling. We neglect those in this thesis.

[2] Nozieres and Pines, 1999

However, there is a class of materials for which the interactions are so strong that the picture of adiabaticity breaks down. This is often the case when d- or f-orbitals are involved. Then the simplest approach is to include the **onsite Coulomb interaction**

$$H_U = U \sum_i n_{i\uparrow} n_{i\downarrow}, \tag{3.3}$$

which leads to the famous **Hubbard model**[3]

$$H_H = -t \sum_{\langle ij \rangle \sigma} c^\dagger_{i\sigma} c_{j\sigma} - \mu \sum_{i\sigma} c^\dagger_{i\sigma} c_{j\sigma} + U \sum_i n_{i\uparrow} n_{i\downarrow}, \tag{3.4}$$

[3] Anderson, 1959; and Hubbard, 1963

where we restricted the hopping to be nearest neighbor only. Figure 3.1 illustrates the elementary physics described by such a Hubbard model on a square lattice.

It is quite embarrassing that even today the physics of the Hubbard model is not fully understood. The first reason lies in the inherent competition between kinetic and potential energy. The kinetic energy is diagonal in momentum space, which suggests we should treat the electrons as waves. The potential energy, however, is diagonal in real space, hence we should consider the electrons as particles. The quantum mechanical **particle-wave duality** reaches its apex of complexity when $zt \approx U$.[4]

[4] The factor z is the coordination number of the lattice, thus zt is proportional to the bandwidth or kinetic energy.

Another reason that the Hubbard model is so poorly understood is the **fermion sign problem**. In numerical analysis this means that one cannot map the model onto a classical probabilistic theory. Analytical progress is difficult since the sign problem implies that wavefunctions are no longer simple product states but rather complicated long-range entangled states.[5]

[5] Liang et al., 1988

Despite these issues, we can construct a microscopic model of a strongly correlated bilayer based on the Hubbard model. The **extended bilayer Hubbard model** contains a kinetic part

$$H_K = -t \sum_{\langle ij \rangle \ell \sigma} c^\dagger_{i\ell\sigma} c_{j\ell\sigma} - \sum_{i\ell} \mu_\ell n_{i\ell} - t_\perp \sum_{i\sigma} (c^\dagger_{i1\sigma} c_{i2\sigma} + h.c.) \tag{3.5}$$

where t is the intralayer hopping, $t_\perp$ is the interlayer hopping and μ_ℓ is the chemical potential per layer. We denote lattice sites by their in-plane index i and their layer number $\ell = 1, 2$. Next to the kinetic part the model contains the onsite interaction

$$H_U = U \sum_{i\ell} n_{i\ell\uparrow} n_{i\ell\downarrow} \tag{3.6}$$

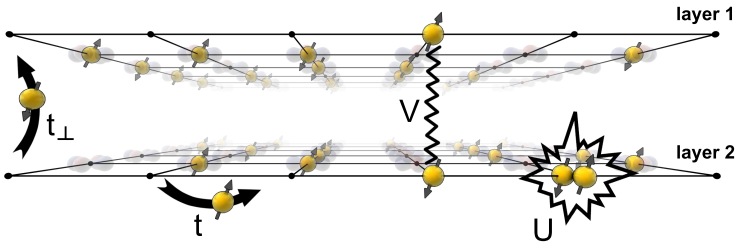

Figure 3.3: The extended bilayer Hubbard model (3.5)-(3.7) describes two layers with in-plane hopping t and interlayer $t_\perp$, onsite repulsion U and interlayer Coulomb interaction V.

and the interlayer interaction

$$H_V = \sum_{ij\sigma\sigma'} V_{ij} n_{i1\sigma} n_{j2\sigma'}. \tag{3.7}$$

A graphic representation of the extended bilayer Hubbard model is shown in figure 3.3.

The occurrence of **interlayer excitons** in this model can be investigated in various limits. Whenever the interactions U and V are relatively weak mean field theory is applicable, similar to how BCS theory describes the pairing of electrons into Cooper pairs.[6] This will be detailed in the next section.

[6] Bardeen et al., 1957

Another limit is the Hubbard model on a bipartite and half-filled[7] lattice with strong interaction U. There the system unambiguously becomes a **Mott insulator**.[8] The electrons are localized and only their spin degree of freedom remains, which in turn order antiferromagnetically. The effective physics can then be expressed in a bosonic spin language, which will be discussed in chapter 4.

[7] Bipartite means I can subdivide the lattice into two sublattices, and every site is only connected to sites on the other sublattice. Half-filling means that there is on average 1 electron per lattice site.

[8] Mott, 1949; Anderson, 1952; and Marshall, 1955

The final approach to the fermionic bilayer Hubbard model is brute force. The Determinant Quantum Monte Carlo technique allows exact computation of several interesting properties of the bilayer Hubbard model, as we will show in section 3.3.

3.2 *The BCS theory of electron-hole pairing*

This section shows an elementary computation, similar to the various **mean field computations**[9] in the literature. Mean field theory, however, grossly overestimates the tendency to form exciton condensates and it surely is not applicable to strongly correlated bilayers. Keeping this in mind, let us now derive electron-hole

[9] Amongst them most notably the prediction of room-temperature superfluidity in Min et al., 2008.

pairing in the bilayer Hubbard model.

The idea of **BCS theory** is to single out the interactions being responsible for the expected order, which is in our case the interlayer exciton condensate with order parameter (3.58). In momentum space, the **order parameter** reads

$$\Delta_{\mathbf{k}} = \frac{1}{2}\sum_{\sigma}\langle c^{\dagger}_{\mathbf{k}1\sigma} c_{\mathbf{k}2\sigma}\rangle \tag{3.8}$$

which is a spin singlet. The interaction that induces exciton condensation scatters excitons from momentum $\mathbf{k}$ to momentum $\mathbf{k}'$. Thus we need to focus on the interlayer interactions

$$H_{V,\mathrm{BCS}} = \sum_{\mathbf{k}\mathbf{k}'\sigma} V_{\mathbf{k}-\mathbf{k}'} c^{\dagger}_{\mathbf{k}1\sigma} c_{\mathbf{k}'1\sigma} c^{\dagger}_{\mathbf{k}'2\sigma} c_{\mathbf{k}2\sigma}. \tag{3.9}$$

The idea of mean field theory is to replace $c^{\dagger}_{\mathbf{k}1\sigma} c_{\mathbf{k}2\sigma}$ in the interaction terms by $\Delta_{\mathbf{k}} + \delta\left(c^{\dagger}_{\mathbf{k}1\sigma} c_{\mathbf{k}2\sigma}\right)$, and then neglect terms of order δ^2. The resulting mean field Hamiltonian is

$$\begin{aligned} H_{MF} &= \sum_{\mathbf{k}\ell\sigma} \xi_{\mathbf{k}\ell} c^{\dagger}_{\mathbf{k}\ell\sigma} c_{\mathbf{k}\ell\sigma} \\ &\quad - \sum_{\mathbf{k}\sigma}\left(t_{\perp} + \sum_{\mathbf{k}'} V_{\mathbf{k}-\mathbf{k}'}\Delta_{\mathbf{k}'}\right)\left(c^{\dagger}_{1\mathbf{k}\sigma} c_{2\mathbf{k}\sigma} + h.c.\right) \\ &\quad + \sum_{\mathbf{k}\mathbf{k}'\sigma} V_{\mathbf{k}-\mathbf{k}'}\Delta_{\mathbf{k}'}\Delta_{\mathbf{k}}. \end{aligned} \tag{3.10}$$

We have introduced $\xi_{\mathbf{k}\ell} = \varepsilon_{\mathbf{k}\ell} - \mu_{\ell}$ as the dispersion minus chemical potential for each layer. This mean field Hamiltonian is quadratic in the fermionic operators and can thus be solved exactly. The dispersion of the quasiparticles depends on the order parameter Δ

$$\begin{aligned} \omega_{\mathbf{k}\pm}(\Delta) &= \frac{1}{2}(\xi_{\mathbf{k}1} + \xi_{\mathbf{k}2}) \\ &\quad \pm\sqrt{\left(\frac{1}{2}(\xi_{\mathbf{k}1} - \xi_{\mathbf{k}2})\right)^2 + \left(t_{\perp} + \sum_{\mathbf{k}'} V_{\mathbf{k}-\mathbf{k}'}\Delta_{\mathbf{k}'}\right)^2}. \end{aligned}$$

The corresponding mean field energy

$$E(\Delta) = \sum_{\mathbf{k}\pm\sigma} \omega_{\mathbf{k}\pm} n_{\mathrm{FD}}(\omega_{\mathbf{k}\pm}) + \sum_{\mathbf{k}\mathbf{k}'\sigma} V_{\mathbf{k}-\mathbf{k}'}\Delta_{\mathbf{k}'}\Delta_{\mathbf{k}} \tag{3.11}$$

needs to be minimized to find a solution for $\Delta_{\mathbf{k}}$.

Up till here the mean field analysis is fairly general: we have not specified the shape of the dispersions $\xi_{\mathbf{k}\ell}$ or the interaction $V_{\mathbf{k}}$. A simple choice is the free electron dispersion[10]

[10] Lozovik and Yudson, 1976

$$\xi_{\mathbf{k}} = \frac{(\mathbf{k}-\mathbf{k}_0)^2}{2m} \tag{3.12}$$

which can be modified to match any lattice, such as graphene's hexagonal lattice.[11] Usually the dispersion is linearized

[11] Dillenschneider and Han, 2008

$$\xi_{\mathbf{k}} = v_F(\mathbf{k}-\mathbf{k}_0) \tag{3.13}$$

around the Fermi level to simplify the computations.[12] One can also introduce spin-orbit coupling which is needed for exciton condensates in topological insulator bilayers.[13] In our case of bilayer cuprates we consider the dispersion generated by nearest neighbor hopping on a square lattice,

[12] Shevchenko, 1976; Lozovik and Sokolik, 2008; Zhang and Joglekar, 2008; Kharitonov and Efetov, 2008; and Min et al., 2008

[13] Seradjeh et al., 2009

$$\xi_{\mathbf{k}1} = -zt\frac{1}{2}(\cos k_x + \cos k_y) - \mu, \tag{3.14}$$

$$\xi_{\mathbf{k}2} = +zt\frac{1}{2}(\cos k_x + \cos k_y) + \mu, \tag{3.15}$$

see figure 3.4.

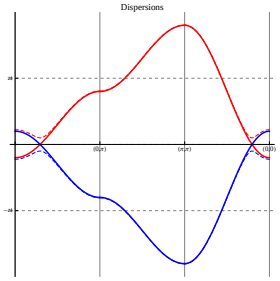

Figure 3.4: Dispersion of the electrons and holes in the absence of any interactions. The red thick line denotes the electron band, the blue thick line is the hole band. When a finite $t_\perp$ is included, a gap opens up around the Fermi surface, and the corresponding upper and lower bands are shown with dashed lines.

The type of interaction can be either nearest neighbor only, screened Coulomb or normal Coulomb. Here we choose for sake of simplicity the nearest neighbor interaction

$$V_{\mathbf{k}} = V. \tag{3.16}$$

With this choice of interaction it becomes reasonable to assume that the order parameter becomes independent of momentum $\Delta_{\mathbf{k}} = \Delta$; this amounts to only local electron-hole pairing. The mean-field energy at $T = 0$ now equals

$$E(\Delta) = 2V\Delta^2 - \frac{2}{N}\sum_{\mathbf{k}}\sqrt{\xi_{\mathbf{k}}^2 + V^2\Delta^2} \tag{3.17}$$

where $\xi_{\mathbf{k}} = \frac{1}{2}(\xi_{\mathbf{k}1} - \xi_{\mathbf{k}2})$. The minimization condition $\partial E/\partial\Delta = 0$ yields the **gap equation**[14]

$$\frac{1}{V} = \frac{1}{2N}\sum_{\mathbf{k}}\frac{1}{\sqrt{\xi_{\mathbf{k}}^2 + V^2\Delta^2}}. \tag{3.18}$$

[14] A convenient way to express the gap equation is to replace the momentum sum by an integral over energy,

$$\frac{1}{V} = \int \frac{D(\varepsilon)d\varepsilon}{2\sqrt{\varepsilon^2 + V^2\Delta^2}},$$

where $D(\varepsilon)$ is the density of states.

Let us pick some relevant parameters and solve the gap equation exactly. The typical hopping energy in cuprates is $t \approx 0.4$ eV. The interlayer hopping $t_\perp$ is set to zero because of the insulating layer that prevents exciton annihilation. A reasonable estimate for the interaction strength is to take it equal to the hopping energy:

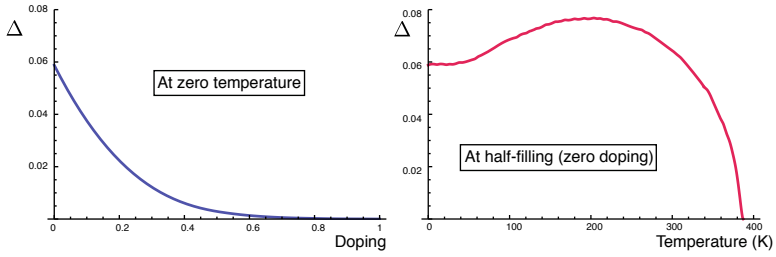

Figure 3.5: The exciton condensate order parameter Δ in mean field theory, found by the gap equation (3.18). **Left:** Δ at zero temperature as a function of doping. Note that zero doping equals half-filling. **Right:** Δ at half-filling as a function of temperature. The exciton condensate is stable up to $T_c \approx 385$ Kelvin.

$V \approx t$. Given these parameters we compute Δ as a function of particle density n at zero temperature, see figure 3.5.

The same minimization procedure can be obtained to find finite temperature behavior of the order parameter. At half-filling ($\mu = 0$) the density of states at the Fermi level is the highest, such that we find there the strongest instability towards exciton condensation. As shown in figure 3.5 the gap reduces with temperature until it vanishes at $T_c \approx 385$ K.

It is within this mean field approach quite easy to find a very large critical temperature. The predictions of room-temperature superfluidity[15] in exciton systems are obtained in this way. One must bear in mind, however, that mean field theory in general overestimates the tendency to order. On top of that, the fact that we are dealing with relatively strong Coulomb interactions makes the theory basically **unreliable**.

[15] Min et al., 2008

Besides the intrinsic problems that mean field theory has, the applicability to strongly correlated bilayers is further reduced because it does not take into account the strong onsite repulsion U. This is an example of an interaction that is not involved in the pairing mechanism, and can only be included perturbatively. Since $U > V$ a perturbative approach is unjustifiable.

We therefore need to resort to numerical approaches that treat the interactions U and V on the same footing as the kinetic energy t.

3.3 *Numerical approach: Determinant Quantum Monte Carlo*

This section is based on Rademaker et al., 2013c.

There are several numerical schemes available to study the Hubbard model. The straightforward manner is exact diagonaliza-

tion,[16] whereby one explicitly constructs the Hamiltonian matrix on a finite size cluster. The problem is that the Hilbert space size diverges exponentially with the system size: a simple 6×6 lattice has already a 69 billion dimensional Hilbert space. The **Determinant Quantum Monte Carlo** (DQMC)[17] technique on the other hand maps the fermionic Hubbard model onto a classical statistical problem, which can then be sampled using standard Monte Carlo methods.

[16] Kaneko et al., 2013

[17] Blankenbecler et al., 1981; White et al., 1989b; and White et al., 1989a

Therefore we first rewrite the kinetic part of the bilayer Hubbard model in a matrix form,

$$H_K = \sum_{ij\ell\ell'\sigma} c^\dagger_{i\ell\sigma} k^\sigma_{i\ell,j\ell'} c_{j\ell'\sigma}. \tag{3.19}$$

If we have two layers of size $N \equiv N_x \times N_y$, the matrix k^σ is a $2N \times 2N$ matrix. The partition sum and the Greens function can now be exactly computed using this k-matrix,

I_{2N} is the $2N \times 2N$ identity matrix.

$$Z \equiv \mathrm{Tr}\left[e^{-\beta H_K}\right] = \det\left[I_{2N} + e^{-\beta k^\uparrow}\right] \det\left[I_{2N} + e^{-\beta k^\downarrow}\right] \tag{3.20}$$

and

$$G^\sigma_{i\ell,j\ell'} \equiv \frac{1}{Z}\mathrm{Tr}\left[c_{i\ell\sigma} c^\dagger_{j\ell'\sigma} e^{-\beta H_K}\right] = \left[I_{2N} + e^{-\beta k^\sigma}\right]^{-1}_{i\ell,j\ell'} \tag{3.21}$$

Notice that the dimension of the k-matrix grows linearly with system size, not exponentially as in the case of exact diagonalization.

To include the interaction terms we rewrite them such that half-filling is always characterized by $\mu = 0$. The onsite repulsion becomes

$$H_U = U \sum_{i\ell} \left[(n_{i\ell\uparrow} - \frac{1}{2})(n_{i\ell\downarrow} - \frac{1}{2}) - \frac{1}{4}\right] \tag{3.22}$$

while the interlayer nearest neighbor repulsion reads

$$H_V = V \sum_{i\sigma\sigma'} \left[(n_{i1\sigma} - \frac{1}{2})(n_{i2\sigma'} - \frac{1}{2}) - \frac{1}{4}\right]. \tag{3.23}$$

Obviously, for the full partition Hamiltonian $H = H_K + H_U + H_V$ we cannot use the result of (3.20). Therefore we need to perform a **Suzuki-Trotter** decomposition. The inverse temperature β is considered as a new dimension and we 'chop up' this imaginary time axis into L pieces,

$$e^{-\beta H} = \left(e^{-\Delta\tau H}\right)^L \tag{3.24}$$

such that $\beta = L \times \Delta\tau$. At each imaginary time slice we split the kinetic part from the interaction parts,

$$e^{-\Delta\tau H} \approx e^{-\Delta\tau H_U} e^{-\Delta\tau H_V} e^{-\Delta\tau H_K} \tag{3.25}$$

which becomes exact in the limit $\Delta\tau \to 0$. We then introduce a discrete **Hubbard-Stratonovich transformation**. On each site and time-slice for each type of interaction we introduce a Hubbard-Stratonovich (HS) field $s(i,\tau)$ which can only take the values ± 1. As a result we decouple the onsite interactions

$$e^{-\Delta\tau U\left[(\hat{n}_\uparrow - \frac{1}{2})(\hat{n}_\downarrow - \frac{1}{2}) - \frac{1}{4}\right]} = \frac{1}{2} \sum_{s=\pm 1} e^{\lambda_U s(\hat{n}_\uparrow - \hat{n}_\downarrow)}, \tag{3.26}$$

where

$$\lambda_U = \operatorname{arccosh}\left(e^{\frac{1}{2}U\Delta\tau}\right). \tag{3.27}$$

A similar decoupling can be formulated for the interlayer interaction V. For each in-plane coordinate i we have six different HS fields $s_\alpha(i,\tau)$: in each layer one associated with the onsite repulsion U and the four possible interlayer interactions for V depending on the particle spin.

The index $\alpha = 1, \ldots, 6$ counts the specific type of HS field.

The advantage of the HS transformation is that the **interaction terms have become quadratic**. Just like we wrote the quadratic kinetic Hamiltonian in terms of a matrix k^σ, we can rewrite the transformed interaction terms using a diagonal matrix $v^\sigma(\tau)$ that depends on the HS fields $s_\alpha(i,\tau)$. Each time slice is therefore represented by the $2N \times 2N$ matrix

$$B_l^\sigma = e^{v^\sigma(l\Delta\tau)} e^{-\Delta\tau k^\sigma}, \tag{3.28}$$

the product of which represents the full evolution among the imaginary time axis

$$M^\sigma = I_{2N} + B_L^\sigma B_{L-1}^\sigma \cdots B_2^\sigma B_1^\sigma. \tag{3.29}$$

The partition sum can be computed exactly by

$$Z = \frac{1}{2^{6NL}} \sum_{s_\alpha(i,\tau)=\pm 1} \det M^\uparrow \det M^\downarrow. \tag{3.30}$$

The equal-time Greens function can be computed by

$$G_{i\ell,j\ell'}^\sigma = \frac{1}{Z} \frac{1}{2^{6NL}} \sum_{s_\alpha(i,\tau)=\pm 1} [M^\sigma]_{i\ell,j\ell'}^{-1} \det M^\uparrow \det M^\downarrow. \tag{3.31}$$

We have thus transformed the bilayer Hubbard model into a Ising-like statistical physics problem. We have $6NL$ 'sites' with ± 1 variables and each possible configuration is weighed by the determinants of the M^σ-matrices.

There are too many configurations to compute (3.30) and (3.31) exactly. Therefore we pick random configurations and compute Z and G and this result will become exact when the number of random configurations approaches infinity. However, one can still do better, via the procedure of **importance sampling**. Thereby we create a Markov chain of configurations, favoring configurations with a larger weight. This is done in such a way that the weight of a configuration is reflected in its occurrence in the Markov chain. In a more precise language, importance sampling requires three steps:

1. Start with a given configuration s.

2. Make a new configuration s' based on the old one, in the present case by randomly changing the six HS fields on a given site and time-slice.

3. Accept this new configuration with a transition probability $T(s \to s')$. This probability must satisfy the detailed balance condition
$$T(s \to s')P(s) = T(s' \to s)P(s') \tag{3.32}$$
where $P(s)$ is the statistical weight of configuration s. Additionally, the function $T(s \to s')$ must satisfy overall ergodicity, which means that there is always a finite chance to get from any initial configuration to any other configuration.

4. 'Measure' parameters of interest, such as the Greens function $[M^\sigma]^{-1}_{i\ell,j\ell'}$, given the configuration at hand. Then go back to step 1 and repeat this sequence until enough measurement points have been accumulated.

5. Do a simple average over the measurement points.

In the **Metropolis algorithm** the new configuration is accepted with probability $T_M(s \to s') = \min(1, P(s')/P(s))$. The **heat bath algorithm** has the transition probability $T_{HB}(s \to s') = P(s')/(P(s) + P(s'))$. Since the importance sampling works best when new configurations are accepted approximately 50% of

the time, in our code we work with a mixture of heat bath and Metropolis prescriptions,

$$T(s \to s') = \gamma \frac{P(s')}{P(s) + P(s')} + (1 - \gamma) \min\left(1, \frac{P(s')}{P(s)}\right) \tag{3.33}$$

where γ is a parameter that we can tune to get the optimal acceptance probability.

3.3.1 *DQMC and the sign problem*

So what happened to the infamous fermion sign problem? The product $\det M^{\uparrow} \det M^{\downarrow}$ can be negative, which implies that we cannot identify it as the weight of a configuration. Instead, we need to define the weight by their absolute value,

$$P(s) = \left| \det M^{\uparrow} \det M^{\downarrow} \right|. \tag{3.34}$$

We then need to measure the **average sign**

$$\text{Sign} = \text{sgn}\left(\det M^{\uparrow} \det M^{\downarrow} \right) \tag{3.35}$$

for each configuration that appears in the Markov chain. Additionally we need to multiply each measurement with the sign of the configuration. In step 5, where we do averaging, we need to divide the result by the average sign.

In the single layer Hubbard model at half-filling the particle-hole symmetry leads to sign-cancellation, such that $\det M^{\uparrow} \det M^{\downarrow}$ is always positive. However, away from half-filling at low temperatures the average sign decreases rapidly. This causes an exponential increase in the errors made since we are dividing by a number that tends to zero. For example, at 15% doping the sign problem prevents us from cooling below 1000 Kelvin: precisely the range where the interesting physics happens.

In our bilayer case it is even worse: the protection guaranteed by particle-hole symmetry is lost because of the interlayer interaction V. Even at half-filling, there will be a sign problem. Our only hope is that the interesting physics, such as exciton condensation, will show up before the average sign drops below ~ 0.2.

3.3.2 *Numerical recipes*

Before we proceed to the results of the DQMC for the bilayer Hubbard model, we need to introduce some numerical tricks that

are needed to make this method work.

For some physical parameters, such as conductivity or pair-susceptibilities, one needs to compute the **unequal time Greens function**

$$G_{i\ell,j\ell'}(\tau,\tau') = \frac{1}{Z}\mathrm{Tr}\left[c_{i\ell\sigma}(\tau)c^{\dagger}_{j\ell'\sigma}(\tau')e^{-\beta H}\right] \tag{3.36}$$

for $\tau > \tau'$. Given a configuration of HS fields we define $\tau = p\Delta\tau$, $\tau' = q\Delta\tau$ and

$$A^{\sigma}_{1} = B^{\sigma}_{p}B^{\sigma}_{p-1}\ldots B^{\sigma}_{q+1} \tag{3.37}$$
$$A^{\sigma}_{2} = B^{\sigma}_{q}B^{\sigma}_{q-1}\ldots B^{\sigma}_{p+1}. \tag{3.38}$$

so that the unequal time Greens function can be computed as

$$G^{\sigma}_{i\ell,j\ell'}(\tau,\tau') = \left[(A^{\sigma}_{1})^{-1} + A^{\sigma}_{2}\right]^{-1}_{i\ell,j\ell'}. \tag{3.39}$$

A major problem in computing the A, M and G matrices lies in the fact that matrix multiplication and inversion is a numerically highly unstable process. One therefore needs to use carefully developed matrix factorization algorithms. Whenever multiplications or inversions seem to become unstable, one needs to perform a **UDR decomposition**[18] of the matrix at hand: U is unitary, D is diagonal and R is an upper triangular matrix with unity pivots. The unstable part of the matrix is now cast in the diagonal part, which needs to be treated carefully.

[18] White et al., 1989b

The construction of the Greens function matrix is in general numerically costly. However, within the importance sampling algorithm one can quickly change the Greens function of the 'old' configuration into the 'new' one. Start with a known Greens Function for both spin species given the HS-fields $s_{\alpha}(i, l\Delta\tau)$ and then change all the six HS fields at site and time-slice $(i, l\Delta\tau)$ yielding a s_{new}. Define

$$\Delta s_{\alpha} = s_{\alpha,\mathrm{new}}(i, l\Delta\tau) - s_{\alpha,\mathrm{old}}(i, l\Delta\tau) = \pm 2 \text{ or } 0. \tag{3.40}$$

Under this change, we note that[19]

$$A^{\sigma} = B^{\sigma}_{l}B^{\sigma}_{l-1}\cdots B^{\sigma}_{1}B^{\sigma}_{L}\cdots B^{\sigma}_{l+1} \tag{3.41}$$
$$\rightarrow \quad A^{\sigma\,\prime} = \left[I + \Delta^{\sigma}\right]A^{\sigma}. \tag{3.42}$$

[19] The equal-time Greens function $G(l\Delta\tau, l\Delta\tau)$ is given by $[I + A^{\sigma}]^{-1}$. The explicit l-dependence is dropped in the following derivation.

The matrix Δ^σ has only two nonzero elements, namely

$$\Delta^{\uparrow}_{i1,i1} = \exp\left[\lambda_U \Delta s_1 + \lambda_V(\Delta s_3 + \Delta s_4)\right] - 1 \quad (3.43)$$

$$\Delta^{\downarrow}_{i1,i1} = \exp\left[-\lambda_U \Delta s_1 + \lambda_V(\Delta s_5 + \Delta s_6)\right] - 1 \quad (3.44)$$

$$\Delta^{\uparrow}_{i2,i2} = \exp\left[\lambda_U \Delta s_2 - \lambda_V(\Delta s_3 + \Delta s_5)\right] - 1 \quad (3.45)$$

$$\Delta^{\downarrow}_{i2,i2} = \exp\left[-\lambda_U \Delta s_2 - \lambda_V(\Delta s_4 + \Delta s_6)\right] - 1. \quad (3.46)$$

The **ratio of weights** between the new $M^{\sigma\prime}$ and the old M^σ equals

$$\begin{aligned} R^\sigma &= \frac{\det[I + A^{\sigma\prime}]}{\det[I + A^\sigma]} \\ &= \det\left[(I + A^{\sigma\prime})G^\sigma\right] \\ &= \det\left[I + \Delta^\sigma A^\sigma G^\sigma\right] \\ &= \det\left[I + \Delta^\sigma (I - G^\sigma)\right] \\ &= \left[1 + (1 - G^\sigma_{i1,i1})\Delta^\sigma_{i1,i1}\right]\left[1 + (1 - G^\sigma_{i2,i2})\Delta^\sigma_{i2,i2}\right] \\ &\quad - G^\sigma_{i2,i1} G^\sigma_{i1,i2} \Delta^\sigma_{i1,i1} \Delta^\sigma_{i2,i2}. \end{aligned} \quad (3.47)$$

Using this formula, we can quickly decide whether we want to accept a change or not, instead of explicitly recalculating the whole determinant. If the change is accepted, we can use a similar trick to update the Greens function. Recall that

$$G^\sigma \to G^{\sigma\prime} = \left[1 + A^\sigma + \Delta^\sigma A^\sigma\right]^{-1}. \quad (3.48)$$

Because the matrix Δ is sparse (it has only two nonzero elements, at i and $i + N$), we can use the **Woodbury matrix identity** to do a fast update of the Greens function. In single layer DQMC one uses the Sherman-Morrison matrix identity, but the interlayer correlations force us to use a generalization. The Woodbury identity amounts to

$$G^\sigma_{ab} \to G^\sigma_{ab} - \sum_{\ell,\ell'} G^\sigma_{a,i\ell} \Delta^\sigma_{i\ell,i\ell} (R^{-1})_{\ell\ell'} (1 - G^\sigma)_{i\ell',b} \quad (3.49)$$

where the spin-dependent R-matrix is given by

$$R_{\ell\ell'} = \begin{pmatrix} 1 + (1 - G^\sigma_{i1,i1})\Delta^\sigma_{i1,i1} & -G^\sigma_{i1,i2}\Delta^\sigma_{i2,i2} \\ -G^\sigma_{i2,i1}\Delta^\sigma_{i1,i1} & 1 + (1 - G^\sigma_{i2,i2})\Delta^\sigma_{i2,i2} \end{pmatrix}. \quad (3.50)$$

Note that the determinant of the R-matrix equals the ratio as defined in equation (3.47). Thus the inverse is trivially given by

$$(R^{-1})_{\ell\ell'} = \frac{1}{R^\sigma} \begin{pmatrix} 1 + (1 - G^\sigma_{i2,i2})\Delta^\sigma_{i2,i2} & G^\sigma_{i1,i2}\Delta^\sigma_{i2,i2} \\ G^\sigma_{i2,i1}\Delta^\sigma_{i1,i1} & 1 + (1 - G^\sigma_{i1,i1})\Delta^\sigma_{i1,i1} \end{pmatrix}. \quad (3.51)$$

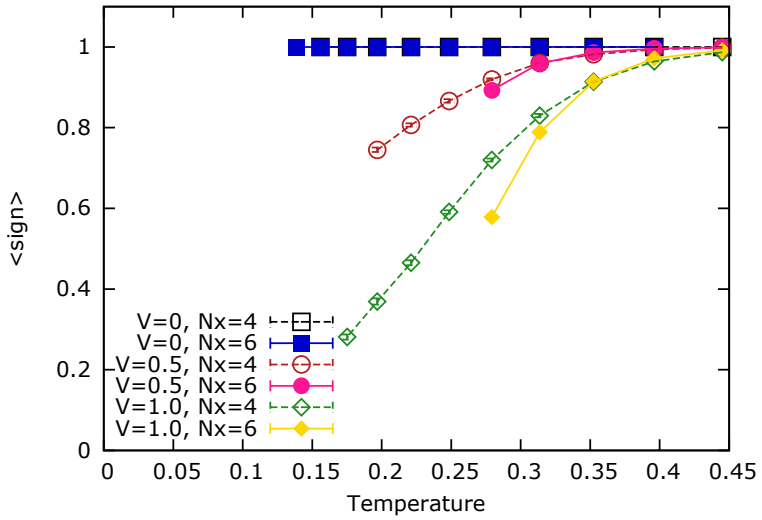

Figure 3.6: The average sign at half-filling for various interlayer interactions V. When $V \neq 0$ the average sign drops rapidly. Parameters are $U = 4t$, $t_\perp = 0.05t$ and $\mu = 0$.

These equations combined yield the full Woodbury update in the case of a bilayer system with interlayer interactions.

The Woodbury identity requires that we consider the equal-time Greens functions $G(\tau, \tau)$ at different imaginary times. A simple trick to get from one time-slice to the next is called **wrapping**,

$$G^\sigma(l+1) = \left[I + B^\sigma_{l+1} B^\sigma_l \cdots B^\sigma_{l+2}\right]^{-1} \tag{3.52}$$

$$= B^\sigma_{l+1} G^\sigma(l) [B^\sigma_{l+1}]^{-1}. \tag{3.53}$$

So for a full update of the Greens function we start at the first time slice. Then we update the HS fields at each site using the importance sampling and the Woodbury identity. Once all sites at a given time-slice are done, we use wrapping to get to the next time-slice. This procedure is repeated until all time-slices are updated. In the mean-time we perform various physically relevant measurements, such as density, spin correlations, etcetera.

Finally we require a numerical recipe for the **error analysis** of the results. A simple root mean-squared error of all configurations is not a good measure.[20] Additionally, the measurements should be independent which is clearly not the case for a Markov chain of configurations. We therefore compute 8 independent Markov chains in parallel, and the error bars are obtained as root mean-squared errors over the averages of each Markov chain. This

[20] For example: if we measure the energy, then the root mean-squared of all independent measurements gives you the specific heat, not the uncertainty in the average energy.

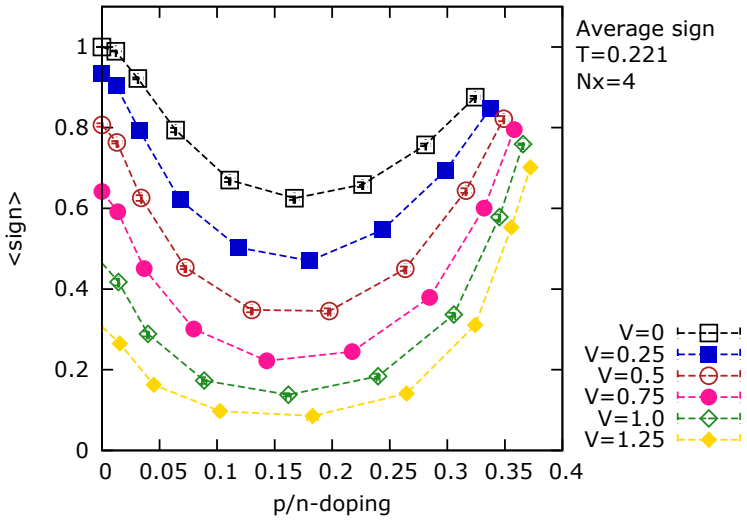

Figure 3.7: The average sign versus density for increasing interlayer interaction V. The temperature is fixed at $T = 0.221$, other parameters are $U = 4t$ and $t_\perp = 0.05t$.

measures the degree to which two independent sampling chains lead to the same average.

3.3.3 *Results on the fermion sign problem*

The applicability of the DQMC method just described is limited by the **measured average sign**, which depends on the specific model parameters such as temperature and interaction strength. We therefore present first our results regarding the average sign, both its value and the impact on the statistical errors on other measurements.

As we briefly mentioned in section 3.3.1, in the absence of the interlayer interaction V at **half-filling** the average sign is always 1 due to particle-hole symmetry. This can be understood by considering the determinants of M^σ for both spin species. Since the Hubbard-Stratonovich fields couple to both the up and down spins, a change of sign in $\det M^\uparrow$ is accompanied by the same sign change in $\det M^\downarrow$. Consequently, at half-filling for $V = 0$ all weights $\det M^\uparrow \det M^\downarrow$ are positive. One can directly infer that this sign cancellation fails when $V \neq 0$, since there are now HS fields that couple to only one type of spin. Indeed, as can be seen in figure 3.6, inclusion of a nonzero interlayer interaction V drastically reduces the sign.

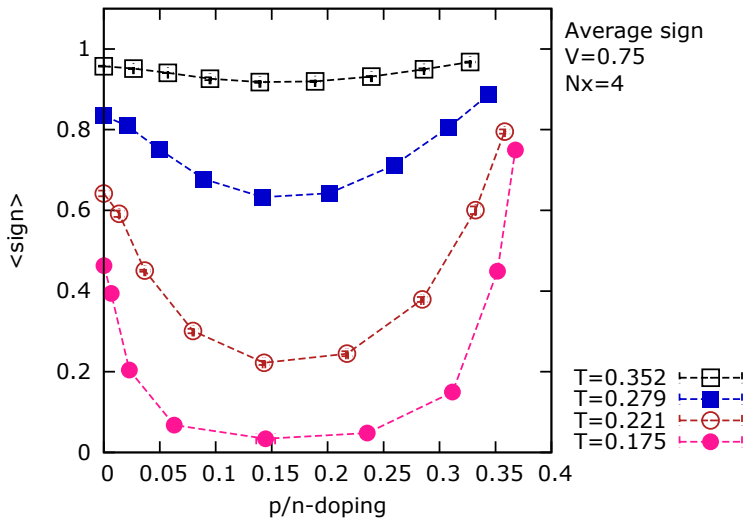

Figure 3.8: The average sign versus density at various temperatures. The interlayer interaction is fixed at $V = 0.75$, other parameters are $U = 4t$ and $t_\perp = 0.05t$. The sign is lowest around $15 - 20\%$ doping.

At **finite densities**, in the case of equal p-type and n-type doping of the two different layers, the average sign is further reduced. Even in the absence of interlayer V, the sign drops so rapidly that the physically interesting regime (with the pseudogap, d-wave superconductivity, etc.) is inaccessible. Figure 3.7 displays how the average sign depends on both doping and interlayer V for a fixed temperature. It is worthwhile to note that the physical temperature corresponding to these parameters is about 900 Kelvins, still an order of magnitude higher than for example the onset of superconductivity in the cuprates. In figure 3.8 we show the average sign as a function of doping for a fixed interlayer coupling $V = 0.75$.

In all cases the sign problem is the **worst around** $15 - 20\%$ p/n**-doping**. Remember that we have one layer doped with holes and another layer doped with the same number of electrons, relative to half-filling. Inclusion of V does not change the qualitative doping dependence of the average sign, it does reduce it significantly.

This is in stark contrast to the suggestion, made in the context of the exciton $t - J$ model of the next chapters,[21] where we consider the limit $V \gg t$, that the sign problem could be reduced upon increasing V. That is based on the idea that the increased interlayer interaction makes it more likely that electrons and holes in the

[21] See Sheng et al., 1996; Wu et al., 2008 and section 4.1.4.

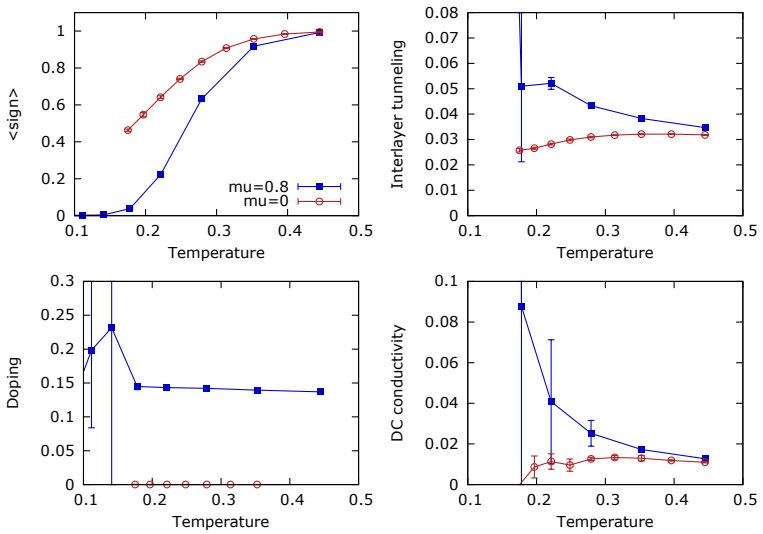

Figure 3.9: Average sign, doping, interlayer tunneling and dc conductivity for $V = 0.75$ and $N_x = 4$ as a function of temperature. Static measurements, such as density and interlayer tunneling, are still reliable as long as the sign > 0.1. The dynamic measurements such as dc conductivity become unstable when the sign < 0.5. For comparison, both $\mu = 0$ and $\mu = 0.8t$ is shown.

two layers move simultaneously, so that the signs of the electrons could be cancelled by the signs of the hole. Based on our DQMC results, this is obviously not the case when the interlayer coupling V is of the same order as t.

Whenever the average sign becomes low, the **uncertainty of measurements increases**. Let us give a rough quantitative estimate of what average sign is still acceptable. Therefore we need to distinguish between two kinds of measurements. **'Static' measurements**, such as the doping and interlayer tunneling, involve only the equal-time Greens function

$$G^{\sigma}_{i\ell,j\ell'} = \langle c_{i\ell\sigma} c^{\dagger}_{j\ell'\sigma} \rangle \tag{3.54}$$

and are more stable than **'dynamic' measurements** involving the unequal-time Greens function

$$G^{\sigma}_{i\ell,j\ell'}(\tau) = \langle T_{\tau} c_{i\ell\sigma}(\tau) c^{\dagger}_{j\ell'\sigma} \rangle. \tag{3.55}$$

In the latter category, we computed the **dc conductivity** based on the current-current correlation function for each layer,

$$\Lambda^{\ell}_{xx}(\mathbf{q}, \tau) = \sum_{i} \langle j_x(\mathbf{r}_{i\ell}, \tau) j_x(0,0) \rangle e^{i\mathbf{q}\cdot\mathbf{r}_{i\ell}} \tag{3.56}$$

Instead of performing the analytic continuation, we approximate the dc conductivity by[22]

[22] Trivedi et al., 1996

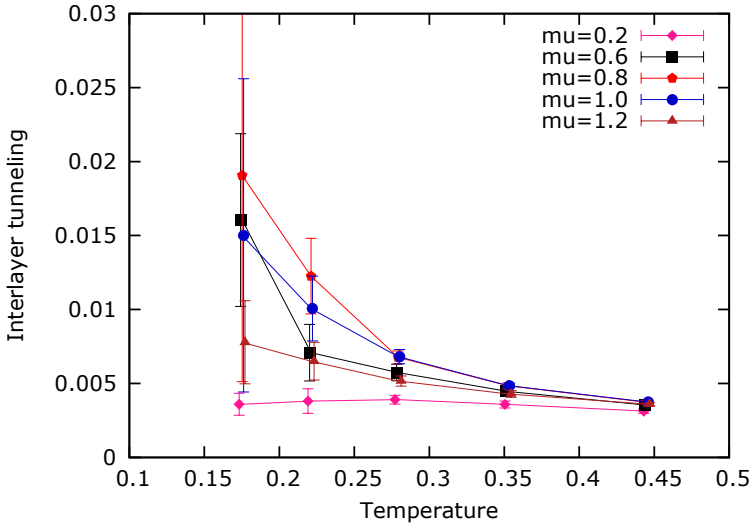

Figure 3.10: Interlayer tunneling at $V = 0.75t$ for $N_x = 4$, relative to the $V = 0$ case. A clear enhancement of the tunneling, which is equal to the exciton condensate order parameter, can be seen around $\mu = 0.8$, where the doping level is approximately 15%.

$$\frac{\pi\sigma_{dc}}{\beta^2} = \Lambda^{\ell}_{xx}(\mathbf{q} = 0, \tau = \beta/2) \tag{3.57}$$

which is valid as long as the density of states is not rapidly varying around the Fermi surface.

In figure 3.9 we show the average sign dependence as a function of temperature for $V = 0.75$, for $\mu = 0$ and $\mu = 0.8$, and relate it to interlayer tunneling, doping and dc conductivity measurements. As long as the average sign is above 0.5, all measurements are statistically trustworthy. Below 0.5, the dc conductivity results have statistical error bars more than half of σ_{dc} itself. Therefore we limit our **dynamical** measurements to regions where the **sign is** < 0.5. Similarly, the error bars on the **static** measurements suggest that we cannot use static data when the average **sign is** < 0.1. This implies that the window for which DQMC is applicable for all doping levels is **limited to about** $\beta < 5$ **and** $V < 1$.

3.3.4 *Exciton condensation*

Our main goal is to investigate whether exciton condensation might occur in the bilayer Hubbard model. Recall that the **order parameter of an interlayer exciton condensate** is[23]

$$\Delta_{\mathbf{k}} = \langle c^{\dagger}_{\mathbf{k}1\sigma} c_{\mathbf{k}2\sigma} \rangle. \tag{3.58}$$

[23] See chapter 2, specifically equation (2.1).

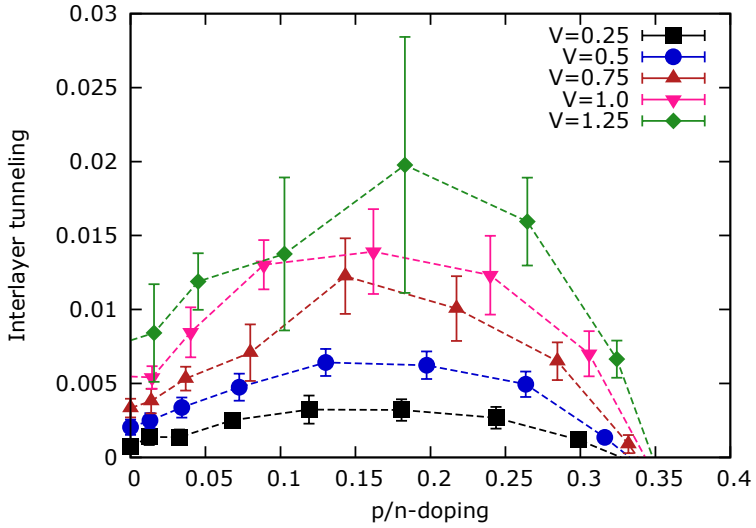

Figure 3.11: Interlayer tunneling for $N_x = 4$, relative to the $V = 0$ case, for all densities and interaction V. A clear enhancement of the tunneling, which is equal to the exciton condensate order parameter, can be seen around the doping level of $15 - 20\%$.

In the presence of strong local interactions **excitons will be formed locally** as well, which means that the electron and hole are above each other. The order parameter becomes independent of momentum and equals

$$\Delta = \frac{1}{N}\sum_i \langle c^\dagger_{i1\sigma} c_{i2\sigma}\rangle. \tag{3.59}$$

The condensate order parameter equals interlayer tunneling,[24] which is directly measurable in experimental set-ups.

[24] Spielman et al., 2000; and Eisenstein and MacDonald, 2004

Within the DQMC method, the interlayer tunneling can be directly read off from the Greens function constructed during the algorithm. The ideal exciton condensate occurs when the interlayer hopping is completely suppressed, $t_\perp = 0$. However, in that case the order parameter calculated in DQMC is identically zero. We **need to include a finite** $t_\perp$, which acts as a symmetry breaking field just like a magnetic field would induce magnetization. The inclusion of a nonzero $t_\perp$ requires us, however, to extrapolate to the perfect $t_\perp \to 0$ case. For this we propose two different schemes.

First, we note that in the absence of an exciton pairing interaction V the interlayer hopping $t_\perp$ will automatically create a doping dependence of the interlayer tunneling. Therefore we separate the contribution to interlayer tunneling that arises due to exciton

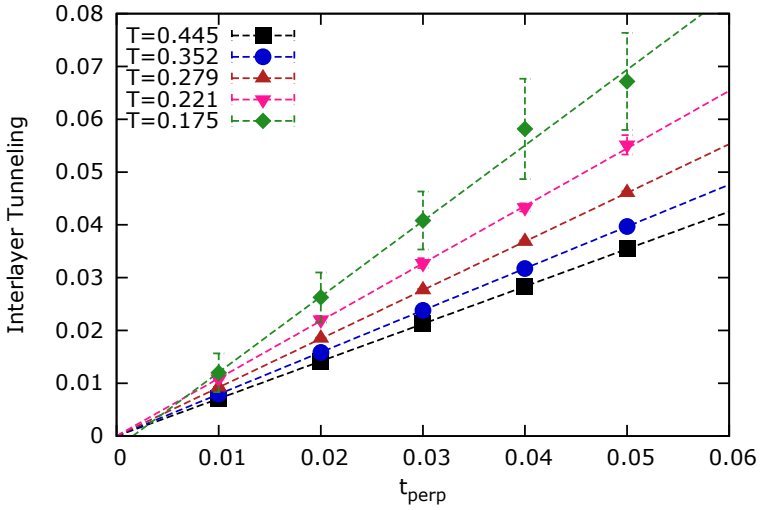

Figure 3.12: Interlayer tunneling at $V = 0.75t$ as a function of $t_\perp$ for $\mu = 1$ and $N_x = 4$. The scaling for $t_\perp$ suggests that there is no exciton condensation.

formation from the part that is already present at $V = 0$. In figure 3.10 we show how this **relative interlayer tunneling** depends on temperature and chemical potential for fixed $V = 0.75$. There is a clear enhancement of the interlayer tunneling around $\mu = 0.8$, which amounts to 15% doping.

At a given temperature of $T = 0.221$ we present the interlayer tunneling as a function of p/n-doping and interlayer interaction V in figure 3.11. The **strongest tendency towards interlayer tunneling is at** $15 - 20\%$ **doping**, for the largest values of interaction V.

Our second strategy to determine the possibility of exciton condensation is to **look at the $t_\perp$-dependence of the interlayer tunneling**. Following the standard BEC/BCS condensation theories,[25] the exciton condensate is represented in the Hamiltonian by the symmetry breaking term

$$-V\Delta \sum_{i\sigma} \left(c^\dagger_{i1\sigma} c_{i2\sigma} + h.c. \right) \tag{3.60}$$

which just adds to the interlayer hopping term $t_\perp$. When $U = V = 0$ we can compute the interlayer tunneling analytically which yields

$$\langle c^\dagger_{i1\sigma} c_{i2\sigma} \rangle \sim \frac{t_\perp + V\Delta}{t}. \tag{3.61}$$

[25] See section 3.2.

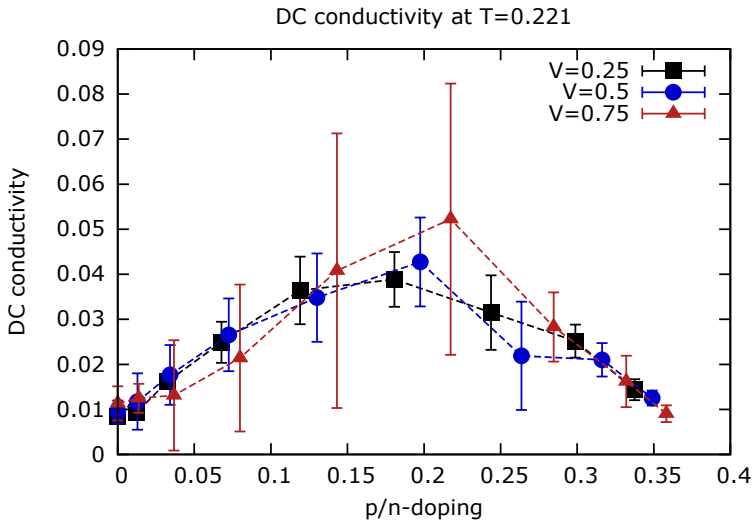

Figure 3.13: The dc conductivity σ_{dc} following equations (3.56)-(3.57) at $T = 0.221$ as a function of doping and V for $N_x = 4$. We only included data points where the error bar on the measurements is less than 50% of σ_{dc} itself. The dc conductivity is the largest at a doping around 20%,

For finite U and V we therefore assume that the interlayer tunneling is a linear function of $t_\perp$, and the order parameter can be found by taking the limit $t_\perp \to 0$. This is done for $V = 0.75$ and $\mu = 1$, parameters for which the interlayer tunneling is the largest, in figure 3.12. As the temperature is lowered the interlayer tunneling increases. However, the scaling behavior as a function of $t_\perp$ suggests that there is **no exciton condensation present**. Unfortunately, due to the sign problem, we cannot go lower in temperatures.

Next to direct measurements of the order parameter, one can **probe related properties of the exciton condensate**. Since in an exciton condensate the charge carriers are bound into charge neutral excitons, it is expected that exciton condensates are **insulating**. Let us therefore look at the conductivity measurements, which are severely limited by the sign problem as pointed out in the previous section. In figure 3.13 we display measurements on the dc conductivity following equations (3.56)-(3.57). The conductivity is largest at a p/n-doping of 15-20%, and fairly independent of the interlayer coupling V.

Instead of the conductivity one can look at the **density of states at the Fermi level**, which is approximated by $G(\mathbf{r} = 0, \tau = \beta/2)$.[26] The density of states at the Fermi level indeed closely follows the

[26] Trivedi and Randeria, 1995; and Nowadnick et al., 2012

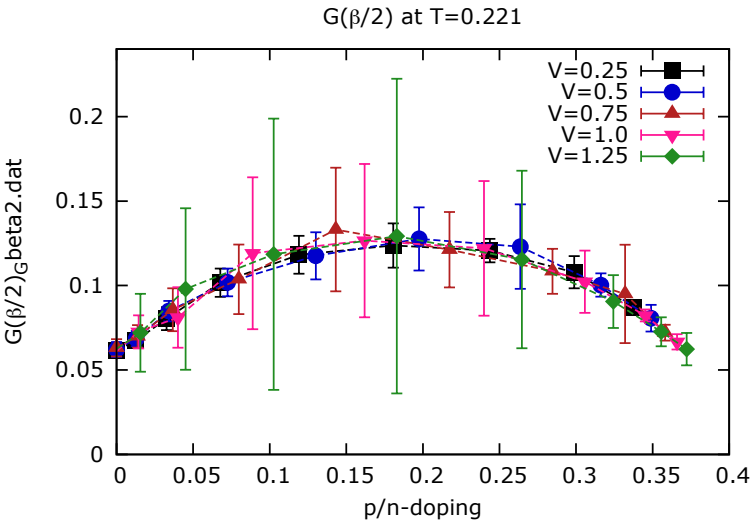

Figure 3.14: The density of states at the Fermi level, approximated by $G(\beta/2)$, at $T = 0.221$ for $N_x = 4$. The density of states is highest around 20% doping, independent of the interlayer interaction V.

p/n-doping dependence of the dc conductivity. Counterintuitively, the increase of conductivity occurs in the region where there is also an increase in the interlayer tunneling. This, together with the $t_\perp$-scaling performed in figure 3.12, rules out exciton condensation at the temperature that are attainable within the DQMC set-up.

In conclusion, we have found no evidence of exciton condensation in the bilayer Hubbard model in the parameter regime accessible by DQMC. However, the increased interlayer tunneling suggests that exciton physics might be relevant for large V, around 15-20% p/n-doping and at temperatures lower than $\beta = 5$.

3.3.5 *Magnetic measurements*

Strong correlations can lead to the localization of electron degrees of freedom, resulting in magnetic correlations. For the Hubbard model on a square lattice this results in **antiferromagnetic order** at half-filling.[27] Experiments on the cuprates show that this antiferromagnetism quickly disappears upon doping.[28] Next to the excitonic physics, we will therefore study the magnetic correlations of the Hubbard bilayer.

[27] See chapter 4.

[28] Imada et al., 1998

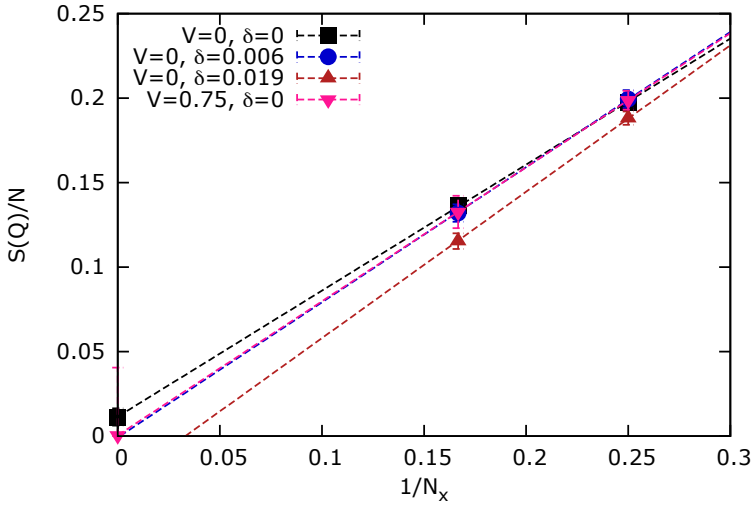

Figure 3.15: Antiferromagnetic correlations at $T = 0.175$ for various V and doping. Only at half-filling ($\delta = 0$) we find antiferromagnetism in the thermodynamic limit.

The antiferromagnetic structure factor in each layer is given by

$$S_\ell(\mathbf{Q}) = \frac{1}{N}\sum_{ij} e^{i\mathbf{Q}\cdot(\mathbf{r}_i - \mathbf{r}_j)} \langle \left(n_{i\ell\uparrow} - n_{i\ell\downarrow}\right)\left(n_{j\ell\uparrow} - n_{j\ell\downarrow}\right)\rangle \qquad (3.62)$$

where $\mathbf{Q} = (\pi, \pi)$ is the antiferromagnetic wave vector. Spin wave theory[29] suggests that $S(\mathbf{Q})$ scales with $1/N_x$ on a finite cluster. The thermodynamic limit $N_x \to$ of $S(\mathbf{Q})$ can be found from a linear extrapolation of the $N_x = 4$ and $N_x = 6$ data, as is done in figure 3.15. Indeed, the antiferromagnetic order is rapidly destroyed as one dopes the layers. However, under the inclusion of V the antiferromagnetic order remains up to $V = 0.75$.

[29] Huse, 1988

Even though the antiferromagnetic order is rapidly destroyed, the **localization of electrons** associated with the strong onsite repulsion U is reduced less drastically by p/n-doping. The local moment, which measures the degree of localization, is defined as

$$m_{i\ell} = \langle \left(n_{i\ell\uparrow} - n_{i\ell\downarrow}\right)\rangle. \qquad (3.63)$$

The site-averaged local moments are shown in figure 3.16. The localization of electrons is for all intents and purposes independent of the interlayer interaction strength V.

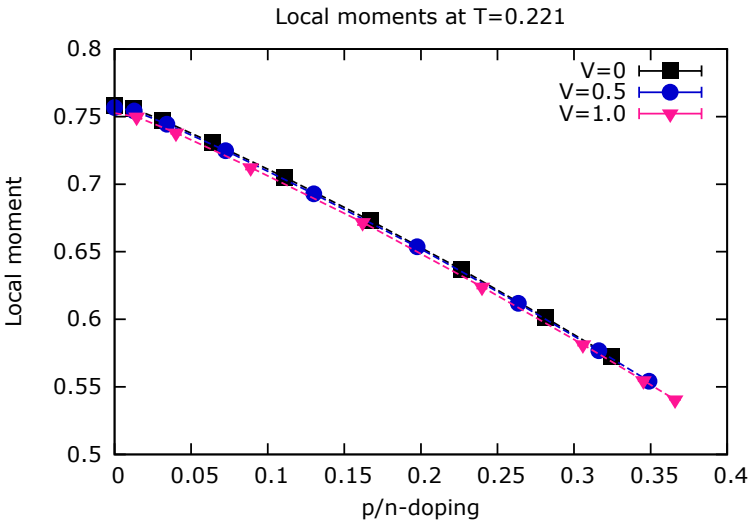

Figure 3.16: The local moments as a function of V and doping at $T = 0.221$ for $N_x = 4$. The localization of electrons is the strongest at half-filling, and almost independent of the interlayer interaction V.

3.3.6 *Conclusion*

The Determinant Quantum Monte Carlo is a brute-force technique that is in principle able to exactly compute physical quantities associated with the Hubbard model. However, the bilayer Hubbard model seems remarkablyunfi unfit for the DQMC approach. Whereas several physical properties such as the conductivity and the magnetic properties are almost independent of interlayer interaction V, the average sign rapidly reduces with increasing V. The desired exciton condensation, measured by interlayer tunneling, is therefore out of reach. Given our data for $\beta < 5$ and $V < 1.25$ we find the **strongest tendency towards exciton condensation around 15-20% doping and at large interaction strength** V. In the next chapter, therefore, we will approach the problem of condensation from the strong coupling limit.